Available online at www.sciencedirect.com
SCIENCE DIRECT®
Thin Solid Films 474 (2005) 19–24
thin solid films
www.elsevier.com/locate/tsf

# Preparation and characterization of Ni–indium tin oxide cosputtered thin films for organic light-emitting diode application

Ching-Ming Hsu*, Jin-Win Lee, Teen-Hang Meen, Wen-Tuan Wu

*Department of Electrical Engineering, Southern Taiwan University of Technology, 1 Nan-Tai St. Yung-Kang City, Tainan Hsien County, 710, Taiwan*

Received 19 January 2004; received in revised form 21 June 2004; accepted 1 August 2004
Available online 11 September 2004

**Abstract**

The characteristics of organic light-emitting diode (OLED) can be improved by the doping of nickel (Ni) into indium tin oxide (ITO) anode. Ni-doped ITO films were synthesized using Ni and ITO cosputter approach. Film properties, such as surface roughness, optical transmittance, sheet resistivity, and surface work function, independent of Ni-doping level were examined. Results show that the Ni-doped ITO films perform lower surface roughness and higher surface work function without scarifying the optical transmittance after thermal annealing at 300 °C. OLED devices with an Al/tris(8-hydroxyquinoline)aluminum/*N*,*N*'-bis-(1-naphthyl)-*N*,*N*'-diphenyl-1,1'biphenyl-4,4'-diamine/ITO/glass structure were fabricated to investigate the effect of the Ni-doped ITO anode. From the *I–V* characteristics of the OLED devices, the threshold voltage can be reduced from 12 to 8 V when the Ni atomic concentration is greater than 1.8%.
© 2004 Elsevier B.V. All rights reserved.

*PACS:* 81.15.Cd; 81.40.-z
*Keywords:* Ni; ITO; OLED; Work function

## 1. Introduction

Since Tang and VanSlyke [1] reported the first high-efficiency heterojunction organic light-emitting diode (OLED), considerable efforts have been made to further improve the optoelectrical performances of OLED to meet the commercialization requirements. The increase of work function of anodes is one way to achieve high-performance OLED devices due to its capability to lower the device turn-on voltage. Indium tin oxide (ITO) is so far the most favourable transparent-conductive anode material for OLED applications, and the studies on the improvement of ITO film properties are still being carried out to optimize the characteristics of OLEDs [2,3]. From the studies reported, surface modification of ITO films has been demonstrated an effective processing to enhance the optoelectrical efficiency of OLEDs [4].

The surface modification of the ITO film is generally conducted by (1) physical surface treatment to obtain low surface roughness [5]. Rough or protrusive surface can generate high local current density and hence the local heating in the OLED active layers, resulting in the deterioration of luminance efficiency and the rapid development of dark spots. ITO films prepared by sputter process usually perform relatively high surface roughness. The physical posttreatment of the ITO film, such as gaseous plasma or ion bombardment [6,7] and chemical–mechanical polishing [8], is necessary. (2) Adjustment of the chemical states to achieve high surface work function [9]. It is well known that the potential barrier between the ITO anode and the organic hole transport layer can be lowered by the elevation of ITO surface work function, and so hole carriers can easily be injected into the OLED active layers at a lower driving voltage. ITO has a work function ranging from 4.2 to 4.7 eV depending on its constituents and the preparation methods. However, work function greater than 5.0 eV is targeted for high-performance OLED devices, and studies on this topic are increasingly important.

* Corresponding author. Tel.: +886 6 2533131, +886 6 2533328; fax: +886 6 2537461.
*E-mail address:* tedhsu@mail.stut.edu.tw (C.-M. Hsu).

0040-6090/$ - see front matter © 2004 Elsevier B.V. All rights reserved.
doi:10.1016/j.tsf.2004.08.005

ITO surface work function can be modulated by changing the constituent of ITO or by the modification of surface chemical states. Of these two approaches, the modification of surface state is considered to be more effective to the surface work function. Several methods have been proposed, including the surface plasma treatment of $O_2$ [10,11], $N_2$ [12], and Cl [13], the immersion of ITO into a surface dipole liquid [14], and the introduction of high work function metals into ITO films [15]. From the literatures reported, majority of the studies on the work function adjustment has been the exposure of ITO surface in energetic gaseous ambient or in liquid solution. However, the potential of adding high work function metals into ITO matrix to yield high surface work function has been increasingly noticed in recent years [15–17].

In this paper, we present a Ni-ITO cosputter approach to fabricate the Ni surface-doped ITO films. The changes in ITO film properties due to the introduction of Ni atoms, such as surface roughness, optical transmittance, sheet resistivity, and surface work function are examined. The effect of the Ni-doped ITO films on the optoelectrical performances of a double heterojunction OLED device is demonstrated.

## 2. Experimental details

The schematic diagram of the Ni-ITO cosputter system is shown in Fig. 1. Dual sputter sources, including a DC power and a radio frequency (RF) power, were used for the deposition of ITO and Ni, respectively. The process chamber was evacuated to a base pressure of $5\times10^{-6}$ Torr before deposition. Sample preparation commenced from the deposition of undoped ITO film onto a glass substrate (50×50 mm in size) at a substrate temperature of 120 °C,

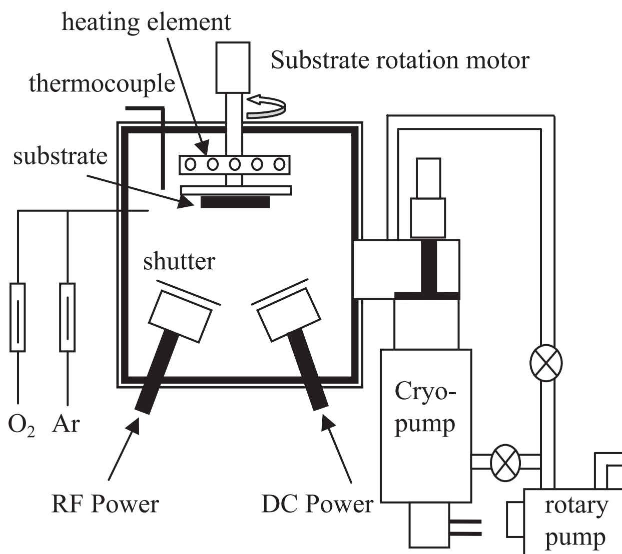


Fig. 1. The schematic diagram of the cosputter system for Ni-doped ITO films. Ni is sputtered using RF power and ITO using DC power.

DC sputter power of 250 W, and process pressure of 3.2 mTorr, which yielded an ITO deposition rate of 30 nm/min. The substrate was placed around 10 cm above an ITO target, which contained 90% of $In_2O_3$ and 10% of $SnO_2$ and was rotated at a speed of 15 rpm to obtain uniform film thickness and Ni-doping concentration. The deposition of the undoped ITO was terminated at the film thickness of 150 nm, which was controlled by time mode, followed by the Ni and ITO cosputtering process to form a Ni-doped ITO top layer of 50 nm. The Ni-doping concentration in the ITO matrix was varied by changing the RF power ranging from 0 to 50 W. Due to the relatively low deposition rate of Ni by RF power compared with that of ITO with DC power, the thickness of Ni-doped ITO was simply determined by the product of the ITO sputter rate and the sputter time. The ITO samples were then thermally annealed in a vacuum ambient at 300 °C for 10 min, followed by the film characterizations using the measuring tools described as follows.

The ITO film thickness and deposition rate were determined using an α-step surface profilometer. Surface roughness measurement was conducted using a contact mode Burleigh METRIS atomic force microscope (AFM) around the central part of the substrate. Surface roughness was measured within a scanning area of 2.5×2.5 $\mu m^2$ at several locations, and the measured roughness exhibits an uncertainty less than 10%. The measurement of Ni atomic concentration in the ITO films was carried out using an Auger Electron Spectrometry (AES; VG MicroLab 310-F). The Ar ion-sputter erosion over an area of 300×150 μm was conducted for depth profiling, and the Ni concentration was determined by the measurement of the Ni LMM peak. The sheet resistivity and optical transmittance of the ITO films were measured using a four-point probe method and a Hitachi 3310 UV spectrometry, respectively. The surface work function of the ITO films was measured using a Kelvin probe method, in which a UV intensity of 500 nm and electron energy between 3.4 and 6.2 eV were employed.

The thermally annealed ITO samples were then used for the synthesis of OLED devices. The OLED device has an Al/tris(8-hydroxyquinoline)aluminum(Alq3)/*N*,*N*'-bis-(1-naphthyl)-*N*,*N*'-diphenyl-1, 1′ biphenyl-4,4′ -diamine (NPB)/ITO/glass structure. The OLED devices were fabricated in a cluster tool consisting of a sample loading/unloading chamber, a resistive thermal evaporation chamber, and an E-beam evaporation chamber. NPB (20 nm) and Alq3 (35 nm) were sequentially deposited using the resistive thermal evaporation onto the ITO-coated substrates through a metal mask. The samples were then transferred into the E-beam evaporation chamber without breaking the vacuum for the deposition of Al electrode (50 nm). A metallic shadow mask was used to form the Al electrode pattern. The synthesized OLED devices were unloaded and immediately characterized using an HP4155B *I–V* meter for the current–voltage (*I–V*) measurement and a Photosearch PR650 CIE (International Commission on Illumination) spectrometry

for the luminance measurement. For the *I–V* characterization, a metal probe was placed on the ITO electrode with a positive bias and another probe on the Al electrode with a negative bias. For the luminance measurement, the CIE spectrometer was placed around 10 cm in front of the sample.

## 3. Results and discussions

### 3.1. Characterizations of the Ni-doped ITO films

#### 3.1.1. Ni concentration in the ITO films

Fig. 2 shows the AES depth profiles of Ni concentration in the Ni-ITO cosputtered ITO films. It can be seen that the Ni concentration increases with the increasing RF sputter power. The averaged atomic concentrations are 1.1%, 1.8%, and 2.6%, respectively, for the RF power of 10, 30, and 50 W. The Ni concentration shows an approximately linear relationship with the RF sputter power, indicating that the incorporation of Ni atoms in the ITO matrix linearly increases with the RF power during cosputtering. This is consistent with the linear relationship between the Ni deposition rate and the RF sputter power as illustrated in Fig. 3. From Figs. 2 and 3, it can be said that the amount of Ni atoms arriving the substrate is linearly dependent on the RF power. The Ni concentration therefore can be directly controlled by adjusting the RF sputter power. Also can be seen in Fig. 2 is that all the Ni concentrations dramatically drop from its averaged value at the depth of 50 nm to zero at the depth of 55 nm. This observation agrees with the earlier description in the experimental details that the thickness of the Ni-doped ITO layer can be well controlled simply by the ITO sputter time mode. It is noted that the dropping of Ni concentration near the film surface is believed due to the establishment of a steady surface state during the Ar bombardment in AES depth profiling.

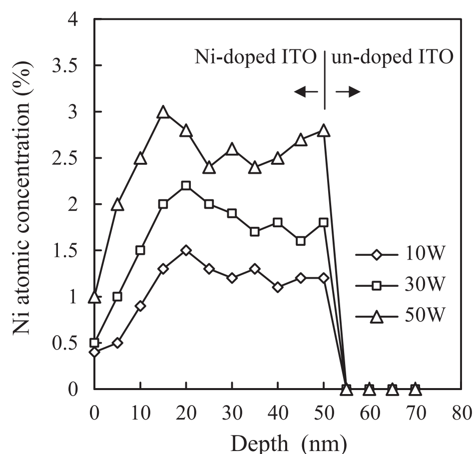


Fig. 2. The AES depth profiles of Ni concentration in the Ni-ITO cosputtered ITO films at various Ni sputter power. The averaged Ni atomic concentration is 1.1%, 1.8%, and 2.6% for Ni sputtered at 10, 30, and 50 W respectively.

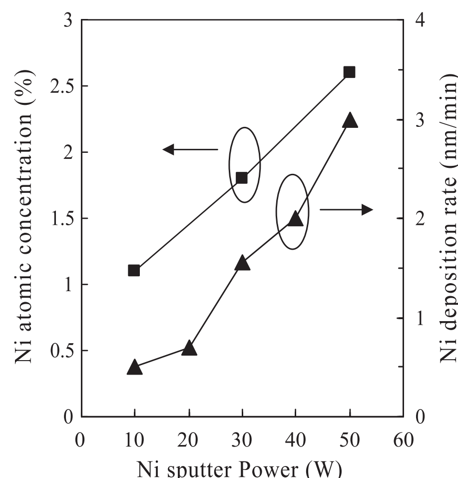


Fig. 3. The Ni deposition rate as a function of the RF sputter power, showing a linear correlation in the power range used.

#### 3.1.2. Surface roughness of the Ni-doped films

Table 1 shows the surface roughness as a function of Ni sputter power for both the as-deposited and annealed ITO samples. It can be seen that in either case, the ITO surface roughness decreases with the increasing Ni sputter power and drops after annealing. The decrease ratio, calculated by dividing the roughness difference by the as-deposited ITO surface roughness, is relatively large for the high Ni atomic concentrations. For example, for the undoped ITO samples, the surface roughness is, respectively, 5.3 nm and 4.8 nm before and after annealing, yielding a decrease ratio of ~10%, whereas that for the Ni(2.6%)-doped ITO is 33% (from 3.3 to 2.2 nm). The slight decrease in surface roughness after annealing for the undoped ITO samples is probably due to that the small and abrupt crystalline grains of the as-deposited ITO films have been broaden and flatten during the annealing. Whereas the large drop in surface roughness for the Ni-doped ITO samples seems to due to the formation of $NiO_x$ phases in the course of annealing [18], which may eliminate the formation of abrupt ITO crystalline.

When the as-deposited surface roughness of the Ni(2.6%)-doped ITO film and the undoped ITO film are compared, a decrease ratio of 40% in surface roughness is found. This evidently indicates that the existence of Ni atom may depress the formation of abrupt ITO crystalline. The surface smoothing effect by the introduction of Ni

Table 1
ITO surface roughness at various Ni sputter power for both as-grown and annealed ITO samples

| Ni sputter power | 0 W | 10 W | 30 W | 50 W |
|---|---|---|---|---|
| Before annealing (nm) | 5.3 | 4.7 | 4.6 | 3.3 |
| After annealing (nm) | 4.8 | 4.1 | 4.0 | 2.2 |
| Roughness decrease ratio (%) | 9.4 | 12.8 | 13.1 | 33.3 |

The roughness decrease ratio was calculated by the roughness difference divided by the roughness before annealing.

atoms is more prominent after annealing with a decrease ratio of 54%. This is probably because more $NiO_x$ can be formed during annealing at high Ni concentration, and the development of sharp crystalline can be reduced.

*3.1.3. Optical transmittance of the Ni-doped ITO films*

The dependence of optical transmittance of the ITO films on the Ni atomic concentration is also of interest. Fig. 4(a) demonstrates the optical transmittance of the undoped and Ni-doped ITO films before and after annealing. The optical transmittances of the ITO films were calculated by averaging the transmittance in the optical spectrum range from 380 to 780 nm. From the figure, it is clear that the optical transmittance decreases as the Ni sputter power increases for both the as-deposited and annealed samples. The optical transmittance drops from 85.7% to 81% for the as-deposited ITO samples and from 90.5% to 88.9% for the annealed ITO samples. The optical transmittance apparently performs less dependence on Ni sputter power for the annealed samples. It is also observed that there is nearly a 10% increase in the optical transmittance for the Ni(2.6%)-doped ITO sample after annealing but only about 5% for the undoped ITO sample. There are two explanations for the above observations, (1) the interstitial atoms in a crystallized film would generate a deformed crystal structure and provide scattering centers. As a result, the incident photons would interact with the scattering center, and the optical absorption can conduct more seriously. The large decrease in the optical transmittance with the increasing Ni sputter power indicates that the Ni photon scattering takes place, and it becomes more prominent when more Ni atoms exist in the ITO matrix. This argument is supported by the fact that the drop in the optical transmittance at long wavelength is less than that at short wavelength according to the measured optical spectra in the visible light region. In the other words, the optical absorption should be partly contributed by the introduction of metallic atoms or the yielded metal oxides which is radiation wavelength-dependent. (2) Defects, such as vacancies and structural imperfections, of crystalline materials can provide the trapping and scattering centers, causing a higher degree of photonic absorption.

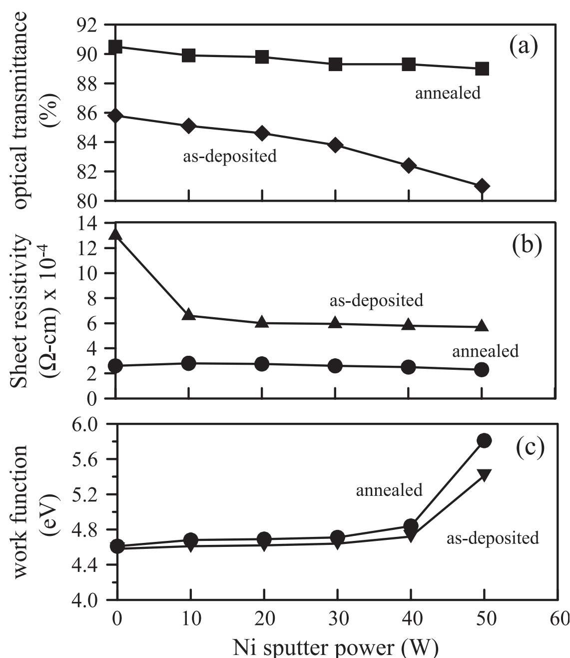


Fig. 4. The dependence of Ni sputter power on ITO film properties (a) the sheet resistivity, (b) the optical transmittance, and (c) the surface work function. Undoped and Ni-doped samples before and after annealing are compared.

From the discussions above, it is reasonable to assume that the defect density in ITO film is higher at high Ni concentration. Therefore, for the as-deposited ITO samples, the Ni-induced high defect density is responsible for the more serious drop in optical transmittance. After annealing, most of the defects in the ITO matrix are repaired, and so the Ni impurity scattering is supposed to be the dominating factor for the deterioration of the optical transmittance. The optical transmittance hence has less dependence on Ni sputter power, because the Ni-induced defects have been largely eliminated. If the Ni-induced surface smoothing effect is also considered, it can be said that the increase in optical transmittance after annealing for the undoped ITO samples is mainly due to the curing of the defects, whereas for the Ni-doped ITO samples, the reduction in the photonic surface scattering may further help to increase the optical transmittance. It is worth to note that the discrepancy in optical transmittance is less than 2%, as the annealed undoped and Ni(2.6%)-doped ITO samples are compared. This gives an idea that the introduction of Ni atoms in the ITO film does not greatly deteriorate the optical transmittance when an appropriate thermal curing process is conducted.

*3.1.4. Sheet resistivity of the Ni-doped ITO films*

Fig. 5(b) shows the sheet resistivity of the as-deposited and annealed ITO films as a function of the Ni sputter power. It can be seen that before annealing, there is a large drop of sheet resistivity between undoped and Ni-doped ITO samples, whereas after annealing, little discrepancy can be found. It seems that the large reduction of sheet resistivity before annealing between the undoped and Ni-doped samples is caused by the additional free electrons introduced by Ni atoms. After annealing, the majority of the defects are repaired for the undoped ITO film. The carrier mobility and concentration may then be comparable to the Ni-doped samples, resulting in the little discrepancy in sheet resistivity with the Ni sputter power. Considering only the Ni-doped samples, the sheet resistivity has slight decrease with the increasing Ni sputter power for both the as-deposited and annealed samples. The negligible dependence of the sheet resistivity on the Ni concentration is considered to be the result of the competition between the Ni atomic scattering and the free electron concentration of Ni atoms. In the other words, Ni atoms in the concen-

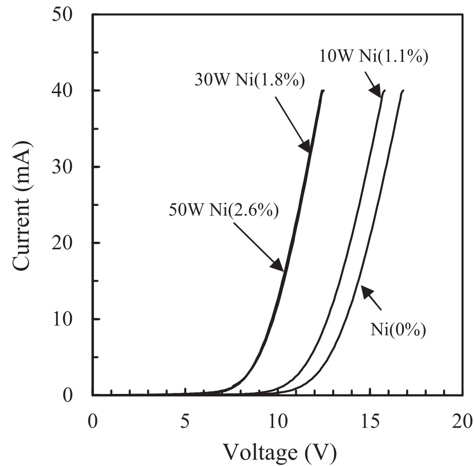


Fig. 5. The *I–V* characteristics of the OLED devices with an Al (50 nm)/NPB (20 nm)/Alq3 (35 nm)/Ni-ITO (200 nm)/glass structure for various Ni sputter power. Prior to the deposition organic layers, all the Ni-doped ITO samples were annealed.

tration range studied (<2.6%) should be still in the form of individual small clusters in the ITO matrix rather than long-range connections between atoms. High Ni concentration would enhance the impurity scattering effect and hence the low carrier mobility, whereas the increase in the amount of Ni atoms could introduce more free electrons. As a consequence, the over whole sheet resistivity of the Ni-doped ITO films slightly decreases with the Ni sputter power. It is also noticed in Fig. 5(b) that the sheet resistivity decreases dramatically after annealing. The curing of the structural imperfection after annealing is believed responsible for this observation provided that the oxygen vacancies are not greatly influenced by the thermal process.

One would expect an ITO film with low optical transmittance and low sheet resistivity due to the adding of Ni atoms into the ITO film. The impurity scattering effect deteriorates the optical transmittance, and the high electron concentration reduces the sheet resistivity. Nevertheless, with well-controlled Ni concentration and proper thermal annealing process, a low sheet resistivity ITO film with high optical transmittance is possible. Table 2 gives the figure of merit of the ITO films, the relationship between the optical transmittance (T)/sheet resistivity (R) ratio, for both the undoped and Ni-doped samples. It is found that the maximum T/R appears at Ni=50 W after annealing, indicating that the optimal film properties can be obtained at high Ni concentration if the optical transmittance and the sheet resistivity are considered at the same weighting. In Table 2, $T^{10}/R$ is also presented to highlight the importance of optical transmittance for OLED applications. The optical transmittance is a factor that directly affects the external efficiency of an OLED device. At Ni=50 W, $T^{10}/R$ has the highest value ($1.4\times10^2$) before annealing but the lowest ($0.21\times10^2$) after annealing, indicating that after annealing, Ni atoms will play a negative role significantly on the optical transmittance. Nevertheless, the adding of Ni atoms into the ITO matrix is still thought to be able to provide a suitable film quality for OLED applications.

#### 3.1.5. Surface work function of Ni-doped ITO films

Fig. 4(c) shows the surface work function, $\phi_s$, of the as-deposited and annealed ITO films as a function of the Ni sputter power. It can be observed that $\phi_s$ rises slightly with the increasing Ni sputter power for PW(Ni) <30 W, and thereafter remarkably increases from 4.81 to 5.80 eV, for example, for the annealed case. The work function of ITO is usually around 4.2–4.5 eV and Ni around 5.2 eV, hence the increase in the work function should be mainly due to the doing of the Ni atoms. The Ni-doping concentration less than 1.8% has little effect on the ITO surface work function, whereas for Ni >1.8%, $\phi_s$ rapidly increases. This could be due to that most of the Ni atoms sit on the vacancy sites in the ITO matrix when its amount is low and may precipitate on the surface when the vacancy sites are completely occupied at high Ni doing. It is also found that $\phi_s$ is elevated after annealing, especially for the Ni-doped ITO films. The formation of $NiO_x$ on the film surface should be responsible for the enhancement as being discussed by Chan et al. [18]. However, the reason why the measured $\phi_s$ for the ITO sample with Ni at 50 W has relatively high value of 5.8 eV is not clear yet. It is suspected that the formation of intermediate phases between Ni and ITO atoms may yield a high ITO surface work function.

### 3.2. Characterizations of the OLED devices

Fig. 5 shows the *I–V* characteristics of the OLED devices at various Ni-doping levels, that is, 0%, 1.1%, 1.8%, and 2.6% which corresponds to the Ni sputter power of 0, 10,

Table 2
The figure of merit, the optical transmittance (T)/sheet resistivity (R) ratio, at various Ni sputter power

| Ni sputter power | | 0 W | 10 W | 20 W | 30 W | 40 W | 50 W |
|---|---|---|---|---|---|---|---|
| T/R | Before annealing (×100) | 12.2 | 13.5 | 14.1 | 14.1 | 13.9 | 13.8 |
| | After annealing (×100) | 32.3 | 32.1 | 32.4 | 34.3 | 35.8 | 40.4 |
| $T^{10}/R$ | Before annealing (×100) | 1.32 | 1.25 | 1.13 | 1.24 | 1.30 | 1.40 |
| | After annealing (×100) | 0.31 | 0.31 | 0.31 | 0.28 | 0.24 | 0.21 |

Both T/R and $T^{10}/R$ are compared.

30, and 50 W. It is quite clear that the *I–V* curve of the OLED devices shifts to the left as the Ni concentration is increased. The threshold voltages are 12, 11, and 8 V for Ni=0, 10, and >30 W, respectively. If these *I–V* characteristics are referred to the ITO work function variation with the Ni concentration in Fig. 4(c), it is apparent that the lowering of the OLED threshold voltage should be mainly contributed from the elevation of ITO surface work function by adding Ni atoms in the surface layers. As mentioned previously, high ITO surface work function will decrease the potential barrier at the ITO/NPB interface, allowing the hole injection from ITO anode at lower driving voltage. However, it is noted that the HOMO energy level of NPB is nominated to be 5.2 eV, lower than the measured value of 5.8 eV at Ni=50 W. This implies that in principle the hole carriers can spontaneously flow into NPB without a driving voltage. Hence, it is suspected that the Ni-doped ITO surface states might be changed when the NPB organic material was being thermally deposited.

The luminance efficiency for the undoped sample and the Ni(2.6%)-doped sample was calculated, and it performs 0.31 and 0.91 lm/W at 250 cd/$m^2$, respectively. The luminance efficiency enhancement is nearly three times in magnitude. The results demonstrate the highly potential of the Ni-doped ITO approach for the application of OLED devices. The Ni-doped ITO effect to the lifetime of OLED devices is also of interest and will be further studied in our future work.

## 4. Conclusions

This report demonstrates that by adding Ni atoms into surface layers, ITO films perform better surface roughness, higher work function, and lower sheet resistivity with only less than 2% loss in the optical transmittance. The existence of Ni atoms around 2% atomic concentration in the ITO top layer can reduce the threshold voltage from 12 to 8 V for OLED devices with an Al/Alq3/NPB/ITO/glass structure. The luminance efficiency is also improved from 0.31 to 0.91 lm/W. The elevation of ITO work function by the Ni doping is proved to be the main factor that enhances the OLED characteristics. The results suggest that the Ni-doped ITO approach is capable of providing high-quality ITO film for the OLED applications.

## Acknowledgment

Authors would like to thank National Science Council (NSC) of Taiwan for the funding support of this project under project number NSC91-2215-E-218-001. Thanks also go to Mr. J. Chen for the measurement of ITO surface work function and Dr. J. Kao in PIDC for the AFM measurement of ITO surface roughness.

## References

[1] C.W. Tang, S. VanSlyke, Appl. Phys. Lett. 51 (1987) 913.
[2] T.Y. Qiu, Y. Gao, L. Wang, D. Zhang, Synth. Met. 130 (2002) 235.
[3] T.P. Nguyen, P.L. Rendu, N.N. Dinh, M. Fourmique, C. Meziere, Synth. Met. 138 (2003) 229.
[4] T.A. Beierlein, W. Brutting, H. Riel, E.I. Haskal, P. Muller, W. Rieb, Synth. Met. 111–112 (2000) 295.
[5] F. Zhu, K. Zhang, B.L. Low, S.F. Lim, S.J. Chua, Mater. Sci. Eng., B, Solid-State Mater. Adv. Technol. 85 (2001) 114.
[6] Y. Qiu, D.Q. Zhang, L.D. Wang, G.S. Wu, Synth. Met. 125 (2002) 415.
[7] H.T. Lu, M. Yokoyama, J. Cryst. Growth 260 (2004) 186.
[8] S. Jung, N.G. Park, M.Y. Kwak, B.O. Kim, K.H. Choi, Y.J. Cho, Y.K. Kim, Y.S. Kim, Opt. Mater. 21 (1–3) (2003) 235.
[9] J.M. Liu, P.Y. Lu, W.K. Weng, Mater. Sci. Eng., B, Solid-State Mater. Adv. Technol. 85 (2–3) (2001) 209.
[10] C.T. Lee, Q.X. Yu, B.T. Tang, H.Y. Lee, Thin Solid Films 386 (1) (2001) 105.
[11] C.C. Wu, C.I. Wu, J.C. Sturm, A. Kahn, Appl. Phys. Lett. 70 (11) (1997) 1348.
[12] C.T. Lee, Q.X. Yub, B.T. Tanga, H.Y. Lee, Thin Solid Films 386 (2001) 105.
[13] S.F.J. Appleyard, M.R. Willlis, Opt. Mater. 9 (1998) 120.
[14] J. Schwartz, E.L. Bruner, N. Koch, A.R. Span, S.L. Bernasek, A. Kahn, Synth. Met. 138 (2003) 223.
[15] A. Wang, N.L. Edleman, J.R. Babcock, T.J. Marks, M.A. Lane, P.W. Nrazis, C.R. Kannewurf, Mater. Res. Soc. Symp. Proc. 607 (2000) 345.
[16] A.J. Freeman, K.R. Poeppelmeier, T.D. Mason, R.P.H. Chang, T.J. Marks, MRS Bull. 25 (2000) 45.
[17] J. Olivier, B. Servet, M. Vergnolle, M. Mosca, G. Gary, Synth. Met. 122 (2001) 87.
[18] I.M. Chan, T.Y. Hsu, F.C. Hong, Appl. Phys. Lett. 81 (10) (2002) 1899.